Available online at www.sciencedirect.com
ScienceDirect
Journal of Nuclear Materials 363–365 (2007) 1315–1322
journal of nuclear materials
www.elsevier.com/locate/jnucmat

Particle balance under global wall saturation in long-pulse discharges of JT-60U

T. Nakano *, N. Asakura, H. Takenaga, H. Kubo, K. Shimizu, H. Kawashima, The JT-60 Team

Japan Atomic Energy Agency, Mukoyama 801-1, Naka-shi, Ibaraki-ken 311-0193, Japan

Abstract

During 30s-ELMy H-mode discharges, the wall-pumping rate decreases with a decay constant of several seconds and then becomes constant. During the constant wall-pumping phase, in discharges with a density of 65% of the Greenwald density, the wall-pumping rate is negative, in other words, outgassing. It has been found that this outgassing rate correlates with an increase in the tile temperature around the outer strike point. In discharges with a density of 80% of the Greenwald density, the wall-pumping rate is positive. Unless a high net deposition rate (>60%) of hydrocarbon is assumed, the positive wall-pumping rate cannot be explained only by the co-deposition of deuterium with carbon even if the outgassing rate is assumed to be zero. The vessel deuterium inventory decreases by 1.1×10^{24} on one experimental day with 17 long discharges. The main chamber wall is suggested as the deuterium source for the decrease of the inventory.

PACS: 52.40.Hf; 52.55.Fa; 52.65.Pp

Keywords: Long-pulse; Steady-state; Particle balance; Wall saturation; JT-60U

1. Introduction

One of the issues in steady-state devices is tritium inventory. In ITER, the safety assessment regulates the upper amount of tritium inventory. To keep the amount of tritium inventory lower than the upper limit, continuous wall-pumping is not permitted. One of the promising solutions for this problem is to exhaust tritium out of the vessel by an active pumping system, such as divertor-pumping.

In devices without cooling system for plasma-facing components (PFC), such as the former Tore Supra (partially the vessel was cooled) [1], Triam-1M [2], JT-60U [3] and HT-7 [4], the wall-pumping rate, which is positive at first, decreases down to a negative rate due to outgassing with an increase of the tile temperature, resulting in a density increase. The density increase can be followed by a plasma disruption in some cases. However, the vessel fuel-particle inventory in these devices decreases due to the outgassing. In contrast, in devices with cooling system for PFC, such as Tore Supra [5] and LHD [6], the wall-pumping rate decreases similarly, and

* Corresponding author.
E-mail address: nakano.tomohide@jaea.go.jp (T. Nakano).

0022-3115/$ - see front matter © 2007 Elsevier B.V. All rights reserved.
doi:10.1016/j.jnucmat.2007.01.221

then, however, it is kept constant at a positive value until the end of discharges. The positive wall-pumping rate keeps the density constant although the vessel fuel-particle inventory continuously increases with discharge duration.

These experimental results indicate that an experimental operation method, in which the density controllability can be maintained and the increase of the vessel fuel-particle inventory can be avoided, has not been established. This is considered to be due to limited capabilities of the devices: pumping speed, tile temperature control, real-time control system, and so on. For instance, the divertor-pumping with a pumping speed comparable to the outgassing speed could avoid the density increase.

In JT-60U, particle controllability with the divertor-pumping system was studied in 30s-ELMy H-mode discharges at a high heating power of 12 MW [7,3]: in repetitive 30s-ELMy H-mode discharges, global wall saturation appeared. During the saturation phase, the plasma pressure at the pedestal region decreased with an increase of the density, and then, the plasma was back-transitioned to an L-mode with an X-point MARFE. During the X-point MARFE phase, the density could not decrease even if the gas-puffing was turned off. In the present study, the strike points were set as close to the pumping slots as possible to utilize the maximum divertor-pumping speed. With this magnetic configuration, a systematic set of data was taken by repeating 30s-ELMy H-mode discharges to obtain a comprehensive understanding of deuterium retention mechanisms.

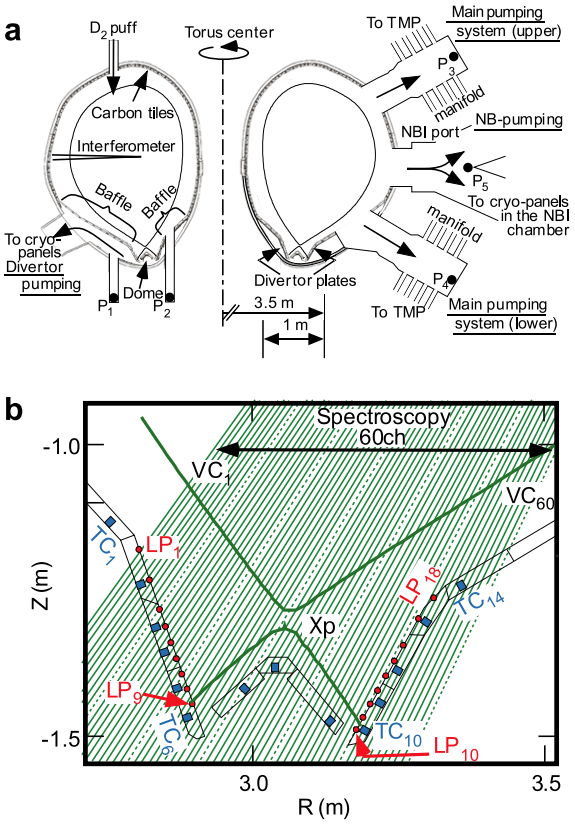

Fig. 1. (a) Schematic view of the poloidal cross-section of JT-60U. The locations of the gas-puffing, the divertor-pumping, the main pumping and the NB-pumping are shown. P_1–P_5 indicate the locations of pressure gauges, and the solid curve the viewing chord of CO_2 laser interferometer (TMP stands for a turbo molecular pump). (b) Expansion view around the divertor. The locations of thermocouples and Langmuir probes and the spectroscopic viewing chords are shown by TC, LP and VC with subscripts, respectively. An *X*-point is indicated by X_p.

2. Experimental

2.1. JT-60U

JT-60U [8] is a large tokamak device with a major radius of 3.5 m, a minor radius of 1.0 m, and a vacuum vessel volume of 114 m^3. Fig. 1(a) and (b) shows, respectively, a schematic view and its expansion view around the divertor of the poloidal cross-section. A W-shaped divertor is composed of baffles, divertor tiles and a dome at the bottom of the vacuum vessel. Carbon tiles cover the whole surface of the inside of the vessel except for some areas for diagnostic windows, heating devices, pumping and fueling systems. Carbon fiber composite (CFC) materials are used for the divertor tiles and some of the dome tiles.

2.2. Diagnostics

The locations of pressure gauges are shown in Fig. 1(a). The pressure gauge P_1 measures the neutral pressure under the baffles, and P_2 in the main chamber. The pressure gauges P_3 and P_4 are positioned in front of the manifolds of the upper and the lower main pumping system, respectively. The pressure gauge P_5 is positioned at the neutral beam injection port. These five pressure gauges are absolutely calibrated for deuterium gas by comparing the pressure measured by these gauges to that measured by an absolutely calibrated gauge (baratron). Also shown are the viewing chord of the CO_2 laser interferometer for line-averaged electron density measurement. In Fig. 1(b), shown are the viewing

chords for CD and C_2 brightness measurement, the locations of Langmuir probes, LP_1–LP_{18}, and the locations of thermocouples, TC_1–TC_{14}, which are positioned below the surface of carbon tiles by 4 mm.

2.3. Pumping and gas-puffing system

As shown in Fig. 1(a), three pumping systems are available: the divertor-pumping, the main pumping and the NB (neutral beam)-pumping system. The divertor-pumping exhausts the neutrals through the pumping slots at the divertor using cryo-panels. The pumping speed was determined by a gas flow test, in which deuterium gas was injected to the vessel at a flow rate from 0.29 Pa m^3 s^{-1} to 8.7 Pa m^3 s^{-1} while only the divertor-pumping was working. The pumping speed, defined as the gas flow divided by the pressure of P_1, was evaluated to be constant, 26 m^3/s, with an error of 20%. The main pumping system consists of the upper and the lower unit at a poloidal section with turbo molecular pumps. The pumping speed of each unit for deuterium gas was evaluated to be, respectively, 6 m^3/s for the pressure at P_3 and P_4, from a pressure decay curve after the gate shutter of the pumping system was unshuttered. The NB-pumping system works only while the neutral beam is NOT injected. During the neutral beam injection, the neutral flux between the vacuum vessel and the NB chamber can be ignored, because the neutral pressure at P_5 is close to that at the entrance of the NB chamber. The pumping speed for deuterium gas was evaluated to be 22 m^3/s for the pressure at P_5 with the same method as the main pumping system.

Deuterium gas is puffed from the top of the vacuum vessel as shown in Fig. 1(a). The gas-puffing rate is determined by a feedback control system to follow a preprogrammed electron density. The error on the gas-puffing rate was estimated to be 10%.

2.4. Long-pulse discharge

Fig. 2 shows the waveforms of the parameters of a 35s-ELMy-H-mode discharge with a density of 65% of the Greenwald density (n_e^{GW}) and a toroidal magnetic field of 2.3 T. The feedback control system of the gas-puffing system kept the line-averaged density constant from 8 s to 28 s. In this period, an ELMy H-mode was maintained with a constant radiation power from the main plasma, and after 20 s, the radiation power from the divertor plasma also became constant. To keep the constant density, the feedback control system reduced the gas-puffing

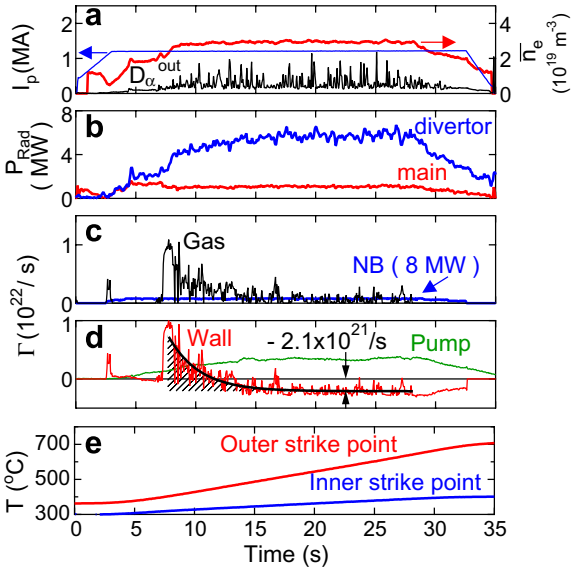

Fig. 2. Waveforms of parameters of a 35s-ELMy-H-mode discharge with a density of 65% of the Greenwald density: (a) plasma current (I_p), the line-averaged electron density ($\overline{n_e}$), (b) radiation power from the divertor and the main plasma, (c) gas-puffing rate, NB fueling rate (injection power: 8 MW), (d) divertor-pumping rate, wall-pumping rate with a regression curve, and (e) temperature around the outer (TC_{10}) and the inner (TC_6) strike point measured by thermocouples (the locations are shown Fig. 1(b)).

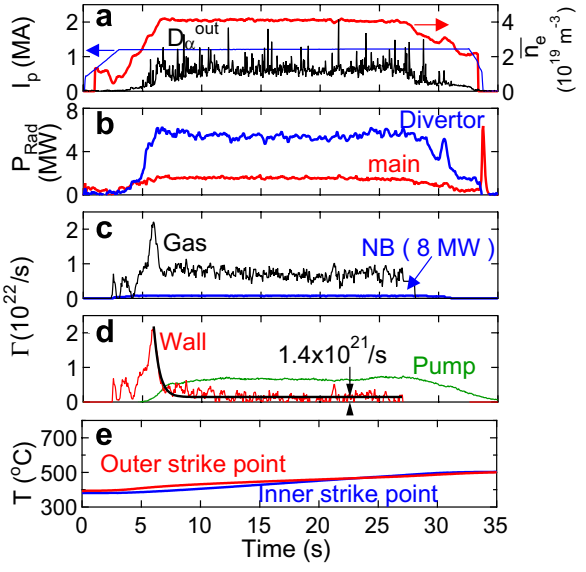

Fig. 3. Waveforms of parameters of a 35s-ELMy H-mode discharge with a density of 80% of the Greenwald density. Meanings of the lines are the same as Fig. 2.

rate to an almost constant rate at 18 s, which is close to the NB fueling rate ($=7\times10^{20}$/s, injection power: 8 MW). The divertor-pumping rate gradually increased, and became constant ($=3.5\times10^{21}$/s) at 18 s.

Fig. 3 shows the waveforms of the parameters of a 35s-ELMy-H-mode discharge with a higher density, 80% of n_e^{GW}. The discharge condition was identical to the low density discharge, except for the density. In the high density discharge, the D_α brightness between ELMs, the radiation power in the main plasma, the gas-puffing rate and the divertor-pumping rate are higher than those in the low density discharge.

3. Analysis

Shown below is the equation used for the particle balance analysis during a discharge. The global deuterium balance inside the surface of the first wall at time t is expressed by the following equation:

$$\frac{d}{dt}N_{plasma}(t) = \Gamma_{gas}(t) + \Gamma_{NB}(t) - \Gamma_{pump}(t) - \Gamma_{wall}(t). \quad (1)$$

Here, $N_{plasma}(t)$, $\Gamma_{gas}(t)$, $\Gamma_{NB}(t)$, $\Gamma_{pump}(t)$ and $\Gamma_{wall}(t)$ indicate, respectively, the number of plasma particles (deuteron), the deuterium gas-puffing rate, the deuterium-fueling rate of NB, the divertor-pumping rate, and the wall-pumping rate. In Eq. (1), the number of neutral deuterium is ignored because of the negligible number, less than ~1% of the plasma particles (deuteron) at most [3], evaluated by SOLDOR simulation [9]. In Eq. (1), the pumping rate by the main pumping system is ignored because it is less than 1% of that by the divertor-pumping. Also, the pumping rate by the NB-pumping system is ignored because this pumping does not work during NB injection as described above.

In the case of $\Gamma_{wall}(t) = 0$, the wall should be considered as globally saturated. The deuterium inventory of all the carbon tiles are not necessarily saturated: it is possible that some tiles are releasing deuterium particles while the others are still pumping.

Integration of $\Gamma_{wall}(t)$ from t_0 to t gives an absolute deuterium inventory at time t if the particle inventory at t_0 is zero. Because, however, it is difficult to determine the absolute deuterium inventory at a certain time, the deuterium inventory relative to that at the start of the first discharge of an experimental day is used, i.e., t_0 is set at the time of the breakdown of the first discharge of an experimental day, to evaluate the day-integrated deuterium balance in Section 4.3.

4. Results and discussion

4.1. Wall-pumping during the steady-state phase

The wall-pumping rate, evaluated by Eq. (1), for instance the low density discharge, shown in Fig. 2(d), decreased with a decay time of $\tau = 2.6$ s (hereafter a transient phase), and became constant ($\Gamma_{wall}^{offset} = -2.1\times10^{21}$/s) (hereafter a steady-state phase), obtained from a regression analysis with an offset-exponential function:

$$\Gamma_{wall}(t) = \Gamma_{wall}^{offset} + \Gamma_{wall}^{0}\exp\left(-\frac{t-t_0}{\tau}\right). \quad (2)$$

In this section, possible mechanisms for the wall-pumping rate during the steady-state phase are investigated.

4.1.1. Negative wall-pumping case

This negative wall-pumping rate, seen in Fig. 2(d), means outgassing from the wall. A possible explanation for this constant outgassing is as follows; the number of deuterium atoms retained in carbon material decreases with increasing material temperature. The gradient of the decreasing curve is regarded as approximately constant in the temperature range from 200 °C to 800 °C [10]. Hence an excess of the deuterium atoms over the saturation amount in the carbon material is released with an increase of the temperature. Furthermore, a constant increase of the material temperature results in a constant excess of the deuterium atoms, and subsequently, the deuterium release rate should be constant. This is the case for the static [10] and the dynamic [11] retention process. Therefore, a constant outgassing rate is expected when material temperature increases at a constant rate. As shown in Fig. 2(e), the tile temperature around the inner and the outer strike point increased at a constant rate. This is considered to be the reason that a constant outgassing rate was observed after 18 s.

Hence, it is expected that the wall-pumping rate depends negatively on the temperature increase rate of a tile, which is predominantly responsible for the outgassing rate. To investigate this dependence, from a set of discharges, the wall-pumping rate during the steady-state phase as a function of the tile temperature increase is plotted in Fig. 4. In the first

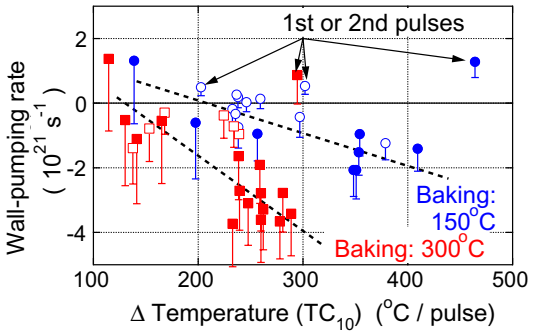

Fig. 4. The wall-pumping rate at the steady-state phase as a function of an increase of tile temperature around the outer strike point. Open and solid symbols indicate the data taken in discharges with an NB heating power of 4 and 8 MW, respectively. Circles and squares indicates the data taken at a baking temperature of 150 °C and 300 °C, respectively. The length of bars only toward negative direction indicates estimated maximum co-deposition rates (see text). The broken lines are to guide readers' eyes.

(and the second in some cases) discharge of the series of the long-pulse discharges, the wall-pumping is usually positive. This is due to overnight glow discharge cleaning, which removes $\sim 1 \times 10^{23}$ deuterium atoms. In other words, the wall saturation appears in the second (or the third in some cases) discharge. Hence, in the following discussion, the data taken in the first and the second discharge are excluded. As shown in Fig. 4, a negative dependence on TC_{10} is seen, although the dependence was not clear if an increase of a tile temperature other than TC_{10} was taken as a horizontal axis. This dependence is due to difference of heating power and density: higher temperature increases are ascribed to higher heating power (8 MW), resulting in higher outgassing rates while lower temperature increases are ascribed to lower heating power (4 MW), resulting in lower outgassing rates. Similarly, higher temperature increases are also ascribed to higher heat load due to lower radiation power in lower density discharges, resulting in higher outgassing rates while lower temperature increases are ascribed to lower heat load due to higher radiation power in higher density discharges, resulting in lower outgassing rates. In addition, an effect of co-deposition gives a negative dependence because higher hydrocarbon flux is expected in higher density discharges than in lower density discharges. This is discussed in Section 4.1.2.

The different dependence of the wall-pumping rate on ΔTC_{10} for a baking temperature of 150 °C and 300 °C is considered to be due to difference of the outer strike position: the outer strike point was positioned closer to TC_{10} at 150 °C than at 300 °C. Thus, at 150 °C, the tile temperature measured by TC_{10} was higher at the end of the discharge even if the temperature at the start of the discharge was lower than that at 300 °C, leading to higher ΔTC_{10} at 150 °C.

4.1.2. Positive wall-pumping case

As shown in Fig. 3(d), the wall-pumping rate of the discharge with a density of 80% of n_e^{GW} is positive ($=1.4 \times 10^{21}$/s). Because the divertor tile temperature increased during the discharge, outgassing is expected. Nonetheless, the positive wall-pumping rate was observed, suggesting another wall-pumping mechanism. As shown in Fig. 5, around the outer strike point, the CD intensity is higher by a factor of 4 in the discharge having 80% of n_e^{GW} than in the discharge having 65% of n_e^{GW}. In addition, the C_2 spectral band intensity is higher by a factor of 9 (not shown). The above observation suggests a wall-pumping mechanism by co-deposition of deuterium with carbon. In order to evaluate the wall-pumping rate due to the co-deposition, the carbon in flux is evaluated as follows; from the measured CD and C_2 photon fluxes, shown in Fig. 5, the chemically sputtered hydrocarbon flux is evaluated, with loss – event/photon coefficients, which convert the CD and C_2 photon fluxes to the CD_4 and C_2D_6 fluxes [13]. Then, the carbon atom flux is calculated by multiplying the number of carbon atoms in these molecules. On the assumption that the sputtered carbons are co-deposited onto the divertor tile with a ratio of

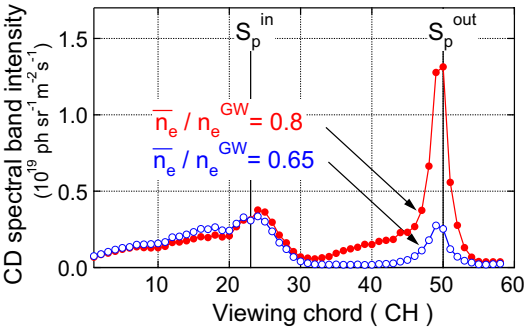

Fig. 5. Distribution of CD spectral band intensity, defined as integral between a wavelength range of 1.5 nm from the band head of $A^2\Delta - X^2\Pi(v = 0–0)$ transition, 430.9 nm. The inner and the outer strike point are indicated by S_p^{in} and S_p^{out}, respectively. The viewing chords is shown in Fig. 1(b).

deuterium to carbon of 0.05 [14] and that the co-deposition layer is never eroded, i.e., 100% net deposition, the maximum co-deposition rate of deuterium during the steady-state phase is estimated, and is shown in Fig. 4 by the length of the bars. The bars are intended to show the range of the wall-pumping rate excluding the co-deposition rate, which depends on the assumed net deposition rate of the sputtered carbon: in the case the net deposition rate is assumed to be 50%, the wall-pumping rate excluding the co-deposition is indicated by the center of the bar. As shown in Fig. 4, with decreasing ΔTC_{10}, the length of the bars becomes long among the data sets particularly for an NB heating power of 8 MW, indicating the co-deposition contributes more to the wall-pumping in high density discharges than in low density discharges.

To explain the measured positive wall-pumping rate, for example shown in Fig. 3(d), a net deposition rate of $\geqslant 60\%$ is required to be assumed even if the outgassing rate is assumed to be zero. This assumed net deposition rate is too high compared with that calculated by the EDDY code [15], which simulates dynamic material erosion by chemical and physical sputtering, impurity transport on the background plasma for the real geometry of the JT-60 divertor determined by the UEDGE code, atomic and molecular processes, and local and prompt redeposition (reflection or sticking of impurity). Hence further deuterium retention mechanisms in addition to co-deposition are suggested.

4.2. Wall-pumping during the transient phase

In all the discharges, a positive wall-pumping rate during the transient phase was observed. This result indicate that the deuterium inventory increases during the transient phase and then it recovers until the start of the next pulse, and that this repeats pulse by pulse. To investigate this repetitive recovery, compared in Fig. 6 is the number of deuterium atoms released after a discharge until the breakdown of the next discharge and the number of deuterium atoms retained during the transient phase of the next pulse, defined as a time-integral of the second term of Eq. (2) from $t = t_0$ to t_{end} (the end of the transient phase): $\int_{t_0}^{t_{end}} \Gamma^0_{wall} \exp(-\frac{t-t_0}{\tau})\,dt$, indicated in Fig. 2(d) by the shaded area, for instance. With some exceptions, the increase of the vessel deuterium inventory during the transient phase is larger than the number of deuterium atoms released between discharges.

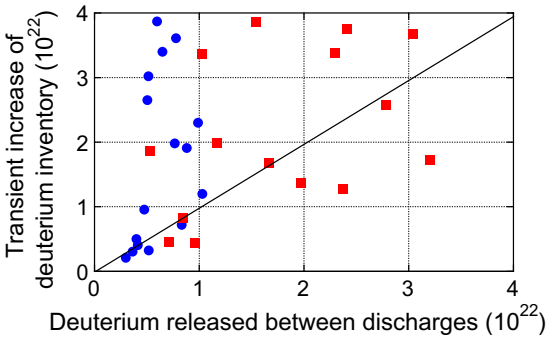

Fig. 6. Comparison of the transient increase of deuterium inventory as a function of the number of deuterium atoms released between discharges. Meanings of the symbols are the same as those in Fig. 7.

This result suggests that another mechanism enhances the deuterium inventory capability in addition to the deuterium release. One possible explanation is an increase of the saturation amount of deuterium in carbon tiles: as already described, the saturation amount of deuterium in carbon material [10] increases with decreasing temperature. Because the tile temperature decreased between discharges, it is expected that the capability to retain deuterium was higher at the start of the discharge than at the end of the discharge. Hence, the recovery of the retention capability between discharges is considered to be due to the deuterium release and the increase of saturation amount of deuterium in carbon tiles.

Next, which tile is responsible for this recovery, or wall-pumping during the transient phase is investigated. Fig. 7 shows the number of pumped deuterium atoms between discharges, normalized for

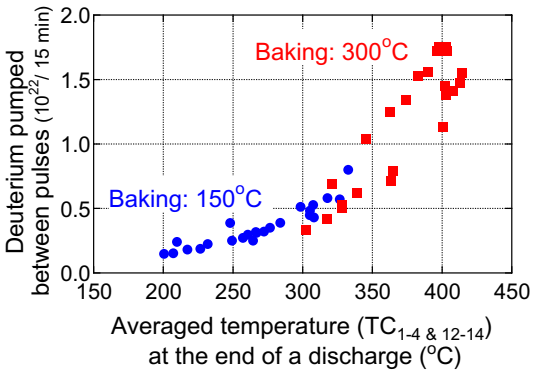

Fig. 7. The number of deuterium atoms pumped between discharges as a function of averaged temperature among seven thermocouples measured at the end of a discharge.

15 min, which is the shortest discharge interval for discharges discussed here because discharge intervals varied. The number of pumped deuterium atoms shows a clear trend in the case it was plotted against the temperature averaged among the seven thermocouples which are positioned at the upper divertor tiles and the baffle tiles. Because the seven temperatures were close (difference: ~50 °C at most) and had similar waveforms, the similar trend was obtained against any one of the seven temperatures. In the case that another tile temperature, for example TC_{10}, is taken as a horizontal axis, no clear dependence was seen. Although this is not necessarily a direct evidence, this result suggests that the deuterium release from the upper divertor tiles and the baffle tiles is one of the contributors to the reduction of the vessel deuterium inventory.

4.3. Day-integrated deuterium balance

Fig. 8 shows the results of a day-integrated deuterium balance analysis. Plotted are the integrated changes of the vessel deuterium inventory during discharges and between discharges. As shown in Fig. 8, the vessel deuterium inventory decreased in discharges with densities of 65% and 70% of n_e^{GW}, decreased at a moderate rate at 75% of n_e^{GW}, and then, did not decrease at 80% of n_e^{GW}. This change of the decrease rate is due to the change of the wall-pumping (or outgassing) rate during a discharge, because the decrease of the deuterium inventory between discharges is essentially constant in comparison to the variation of wall-pumping during a discharge. As already pointed out, the change of the decrease rate is considered to be due to a low outgassing rate due to the small increase of the tile temperature and an increase of co-deposition rate in high density discharges. Eventually, the vessel deuterium inventory decreased by 1.1×10^{24}.

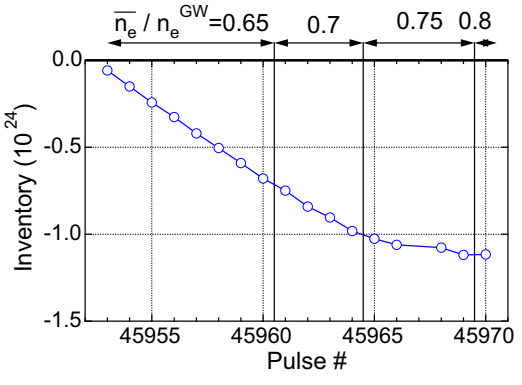

Fig. 8. Vessel deuterium inventory as a function of pulse number.

A possible deuterium source for this decrease of the deuterium inventory is considered to be the main chamber wall: the outer divertor tile is considered to be saturated in ~0.1 s [12] due to the high deuterium flux, and some fraction of retained deuterium atoms are considered to be removed during a discharge due to the increase of its temperature. Because the saturation and the removal are repeated pulse by pulse, the local deuterium inventory at the outer divertor tile is not considered to contribute to the day-integrated vessel deuterium inventory. This is the case for the upper divertor tiles and the baffle tiles, as already discussed. Hence, another deuterium source, for example, the main chamber is suggested. The deuterium inventory in the main chamber wall is estimated to be large enough to explain the decrease of the deuterium inventory [16]. Furthermore, the surface temperature of the main chamber wall increased by 20 °C during a discharge, leading to outgassing. These support the hypothesis that the source for the decrease of the deuterium inventory is the main chamber wall.

5. Summary and conclusions

In order to investigate potential deuterium retention mechanisms, the wall-pumping rate, evaluated by the particle balance analysis, was investigated for a systematic set of data. The wall-pumping rate decreased with a decay constant of several seconds (transient phase) during a discharge, and then became constant (steady-state phase).

The transient wall-pumping was due to the recovery of the vessel deuterium inventory between discharges: the amount of the inventory decreased by releasing deuterium and the capacity to retain deuterium increased due to a decrease of the tile temperature. The strong correlation between the temperature at the upper divertor and the baffle tiles and the number of deuterium atoms released between discharges suggests that the transient wall-pumping is due predominantly to the upper divertor tiles and the baffle tiles.

During the steady-state phase, in discharges with a density lower than 80% of n_e^{GW}, the wall-pumping rate was negative, in other words, outgassing. It was found that this outgassing rate correlated with an increase in the tile temperature around the outer strike point. This is because the decrease of the

saturation amount in the carbon material as a function of the material temperature has an approximately constant gradient [10,11].

In discharges with a density of 80% of n_e^{GW}, which were performed later in order, the wall-pumping rate was positive ($=1.4\times10^{21}$/s). To evaluate the co-deposition rate, the hydrocarbon flux was measured spectroscopically. On the assumption that the ratio of deuterium to carbon in the deposition layer is 0.05 [14], the net deposition rate of the hydrocarbon of 60% is necessary to explain the wall-pumping rate of 1.4×10^{21}/s. However, this net deposition rate is higher than the rate calculated by the local carbon transport simulation code [15]. The net deposition rate should be investigated further experimentally, for example, by a QMB technique.

A possible deuterium source, which explains the decrease of the day-integrated deuterium inventory ($=1.1\times10^{24}$), is suggested to be the main chamber wall; because the outer divertor tile repeats being saturated and depleted pulse by pulse, due to the high deuterium flux and the increase of the temperature, the local deuterium inventory at the outer divertor tile is not considered to contribute to the day-integrated vessel deuterium inventory. This is the case for the upper divertor tiles and the baffle tiles. In contrast, the deuterium inventory in the main chamber wall is estimated to be large enough and the outgassing is expected due to the temperature increase by 20 °C in one pulse. Hence, the main chamber wall is suggested as a possible deuterium source.

References

[1] C. Grisolia et al.The Tore Supra Team, J. Nucl. Mater. 266–269 (1999) 146.
[2] M. Sakamoto, S. Itoh, et al., Nucl. Fusion 42 (2002) 165.
[3] T. Nakano, N. Asakura, et al., Nucl. Fusion 46 (2006) 626.
[4] X.Z. Gong, J. Nucl. Mater., these Proceedings.
[5] E. Tsitrone, C. Brosset, et al., in: Fusion EnergyProceedings of the 20th International Conference Vilamoura, 2004, IAEA, Vienna, 2004, CD-ROM file EX-10/2.
[6] S. Masuzaki, T. Morisaki, et al., J. Nucl. Mater., these Proceedings, doi:10.1016/j.jnucmat.2007.01.028.
[7] H. Takanaga, N. Asakura, et al., J. Nucl. Mater. 337–339 (2005) 802.
[8] H. Kishimoto, S. Ishida, et al., Nucl. Fusion 45 (2005) 986.
[9] K. Shimizu, T. Takizuka, et al., J. Nucl. Mater. 313–316 (2003) 1277.
[10] W. Moller, J. Nucl. Mater. 162–164 (1989) 138.
[11] K. Matsuhiro, M. Isobe, et al., in: Fusion Energy, Proceedings of the 18th International Conference Sorrento, 2000, IAEA, Vienna, 2000, CD-ROM file FTP1/22.
[12] H. Takenaga, T. Nakano, et al., Nucl. Fusion 46 (2006) S39.
[13] T. Nakano, T. Tsuzuki, et al., in: Proceedings of the 32nd European Physics Society Conference on plasma Physics, Tarragona, P1-005, 2005.
[14] T. Tanabe, Fusion Eng. Des. 81 (2006) 139.
[15] K. Oya, et al., J. Nucl. Mater., these Proceedings, doi:10.1016/j.jnucmat.2007.01.282.
[16] K. Masaki, T. Tanabe, et al., in: Fusion Energy, Proceedings of 21st International Conference Chengdu, 2006, IAEA, Vienna, EX/P4-14, ISBN 92-0-100907-0/ISSN 0074-1884.